Line Inductance Stability Operation Domain Assessment for Weak Grids With Multiple Constant Power Loads

Wang, Rui; Sun, Qiuye; Ma, Dazhong; Qin, Dehao; Gui, Yonghao; Peng, Wang

Published in:
I E E E Transactions on Energy Conversion

DOI (link to publication from Publisher):
10.1109/TEC.2020.3021070

Publication date:
2021

Document Version
Accepted author manuscript, peer reviewed version

Line Inductance Stability Operation Domain Assessment for Weak Grids With Multiple Constant Power Loads

Wang Rui, *Student Member, IEEE,* Sun Qiuye, *Senior Member, IEEE,* Ma Dazhong, *Member, IEEE,* Qin Dehao, *Student Member, IEEE,* Gui Yonghao, *Member, IEEE,* Wang Peng, *Fellow, IEEE*

***Abstract*—Weak grids are gaining considerable attention since power generation resources are remote from constant power loads (CPLs), which results in low-frequency/harmonic oscillation. Meanwhile, due to the play and plug demand of modern power system, the line inductance of weak grids often changes, which is also regarded as the variation regarding short circuit ratio (SCR). Based on this, the conventional impedance-based stability operation point assessment approaches should be expanded into stability domain assessment approach considering the line inductance variation. Therefore, the stability-oriented line inductance stability domain assessment approach for weak grids with CPLs is proposed in this paper. Firstly, the source impedance matrix of weak grid and load admittance matrix of CPLs are separately built. Secondly, an improved stability forbidden domain criterion is proposed through related mapping transformation process, which has lower conservatism than two previous improved stability criteria. Thirdly, the improved stability forbidden domain criterion is switched into the condition that the intermediate matrices are Hurwitz. Meanwhile, the line inductance stability domain is directly obtained through these intermediate matrices and guardian map theory. Finally, the simulation and experiment results illustrate that the proposed approach has less conservatism and high efficiency.**

***Index Terms*—weak grid, stability domain, intermediate matrix, guardian map theory.**

I. Introduction

WEAK grids have widely appeared in the areas where the loads are located far away from the centers of power supply, such as rural areas, islands, boards, vehicle charging stations and so on. Interaction between the weak grid and the load, nevertheless, always causes the instability issue and low-frequency/harmonic oscillation in the real applications [1]-[2]. Furthermore, the weak grid is becoming increasingly complex, incorporating distributed renewable energy sources, various loads and so on. For researching the stability issue of the cascaded system, the short circuit ratio (SCR, SCR$\approx 1/L_g$ [p.u.]) is widely utilized to assess the strength of the cascaded system, and the weak grid is further emulated through the ideal voltage source in series with one line impedance [3]. Meanwhile, the loads are always interfaced through the tightly regulated power electronics converters, and operate as constant power loads (CPLs) with negative impedance characteristic, which causes the cascaded system to be more prone to instability in electromagnetic timescale [4]-[5]. Due to the play and plug characteristic of modern power system, the SCR of weak grids is always changed, which causes the continual variation of the equivalent line inductance. It is advisable that the conventional impedance-based stability operation point assessment approaches are expanded into the stability domain assessment approach considering the line inductance variation.

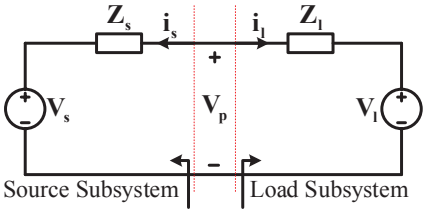

Fig. 1: Thevenin equivalent source/load subsystem model.

The impedance-based approaches were widely applied to analyze the stability issue, and it was based on the return-ratio matrix between source subsystem output impedance matrix ($\mathbf{Z_s}$) and load subsystem input impedance matrix ($\mathbf{Z_l}$) for the cascaded system depicted in Fig. 1 [6]-[7]. The application of the impedance-based approach was traced back to 1976 by Middlebrook, where this approach was applied to design the input filters of dc-dc power converters [8]. Meanwhile, J. M. Undrill, et al analyzed the sub-synchronous oscillations of power systems through the impedances of generators and the transmission network [9]. Moreover, the impedance-based approach was widely studied to assess the small-signal stability of the AC or DC power systems. Thereinto, the conventional Nyquist Criterion (NC) was utilized to identify the DC system stability, and the impedance models in the synchronous reference frame and stationary reference frame were separately established to identify AC system stability through Generalized Nyquist Criterion (GNC) [1], [3]. According to the

This work was supported by National Key Research and Development Program of China (2018YFA0702200), National Natural Science Foundation of China (61773109, 6143304), Major Program of National Natural Foundation of China (61573094). (*Corresponding authors: Sun Qiuye; Ma Dazhong*)

Wang Rui, Sun Qiuye and Ma Dazhong are with the Northeastern University, Liaoning, 110819, China. And Wang Rui is also with the Nanyang Technological University, 637141, Singapore. (e-mail: 1610232@stu.neu.edu.cn; sunqiuye@ise.neu.edu.cn; madazhong@ise.neu.edu.cn.)

Qin Dehao is with the Clemson University Restoration Institute, Clemson University, South Carolina, 29405, USA. (e-mail: dehaoq@clemson.edu.)

Gui Yonghao is with the Automation & Control Section at the Dept. Electronic Systems, Aalborg University, 9220 Aalborg, Denmark. (e-mail: yg@es.aau.dk.)

Wang Peng is with the Nanyang Technological University, 637141, Singapore. (e-mail: epwang@ntu.edu.sg.)

different application cases, several improved impedance-based approaches were proposed [10]-[14]. For the cascaded system with bidirectional power flow feature, the sum type criterion was proposed in [10]. For numerous grid-tied inverters system, the line impedance robust stability identification approach was proposed in [7]. For the cascaded system with mirror frequency coupled feature, the apparent impedance approach, harmonic-state-space (HSS) approach and harmonic-transfer-function (HTF) approach were separately presented in [11]-[13]. For making sure that characteristic values at origin and right half-plane of the impedance matrix were neglected, the inverse Nyquist stability criterion was proposed in [14]. Since NC and GNC are very complex, they are not suitable to supply the guidance for power system designers [15]. Numerous researches were proposed to obtain the improved stability criteria to remove the complex NC or GNC progress and reduce the relative computational burden, which was divided into two series improved stability criteria [15]-[17]. One series improved stability criteria were based on the matrix norm, which were divided into four categories, *e.g.*, the singular-value, the G-norm, the infinity-norm and infinity-one-norm criteria [15]. Another series improved stability criteria were based on the forbidden region [16]-[17]. Undeniably, the artificial conservatism would be introduced in these two series criteria. Therein, there are two main drawbacks for high conservatism. (*i*) The high conservatism will cause inaccurate stability analysis results. For example, the system may be regarded as an instable system in the light of the identification conclusion obtained through criterion with high conservatism. However, the real system is stable. (*ii*) The obtained stability line inductance stability operation domain will be reduced, which is not conductive to design of the power system. Besides, all the above impedance-based approaches focused more on the stability operation point assessment, and from the viewpoint of the computational burden, it is not suitable for providing line inductance stability operation domain for power system designers. There is no doubt that the stability operation domain can also be obtained through point-by-point impedance-based method. However, thousands of generalized Nyquist curves need to be drawn, and each generalized Nyquist curve need to be observed by human, resulting in a huge workload. Therefore, this paper proposes an impedance-based approach to analyze the line inductance stability domain. This approach is also regarded as the robust stability assessment approach regarding line inductance. If power system engineers design the weak grid, the equivalent line inductance or SCR can be extended from a single stability point to a certain stability domain.

In order to give the line inductance stability domain, this paper proposes a stability-oriented line inductance stability domain assessment approach for weak grids with multiple CPLs. Main contributions of this paper are provided below:

1) Constitute an improved stability forbidden criterion for the cascaded system using the related mapping transformations. The criterion has lower conservatism than two series of previous improved stability criteria in [15]-[16];

2) Define three intermediate matrices to describe the stability domain so that the solving process of the line inductance stability domain is switched into the condition that at least one of these three intermediate matrices is Hurwitz, which provides an indispensable preprocessing for obtaining the line impedance stability domain;

3) Propose stability-oriented line inductance stability domain assessment approach with low computational burden, which is based on intermediate matrices and guardian map theory, to directly obtain the line inductance stability domain, supplying the robust stability assessment criterion regarding line inductance.

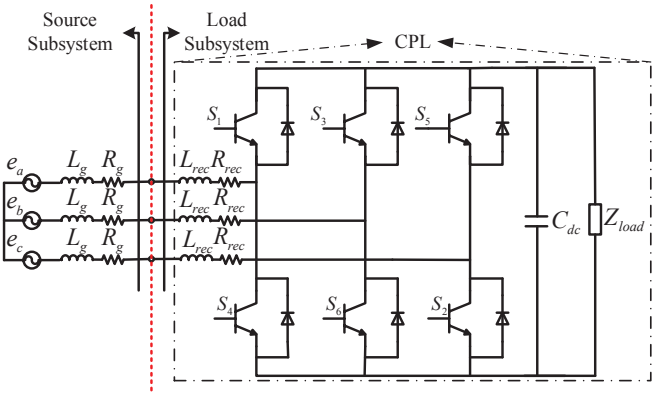

Fig. 2: System configuration of the three-phase weak grid.

II. Terminal Characteristics Modeling of the Three Phase Weak Grid

In rural areas, CPLs are always supplied energy through the weak grid, such as AC distributed power systems, AC-busbar PEV charging station systems and so on [15], [18]-[19]. Therein, the above-mentioned weak grid is able to be equivalent to the system configuration shown in Fig. 2 [15]. Therein, the detailed controller architecture of the constant power load is shown in Fig. 3 [20]. The CPL type in this paper is the tightly regulated power electronics converter load. In general, the regulated power electronics converter is controlled by the traditional current/voltage double-loop controller. Therein, the phase-locked-loop (PLL) is widely applied to acquire the three-phase angular frequency in the $d-q$ frame. According to the literature [2], there are two main improved structure, *i.e.*, PLL structure based on transport delay with phase error compensation and orthogonal system generator second order generalized integrator (SOGI). As mentioned in literature [2], regardless the PLL structure chosen, a small signal approach has been pursued, which can be represented as $G_{PLL}(s)$. Thus, this paper provides a widely adopted PLL structure, which has been shown in Figure 4 of the literature [19]. The three-phase angular frequency is provided as follows:

$$\omega = G_{PLL}(s)\, V_{cq}, \tag{1}$$

where, $G_{PLL}(s)$ is the PLL proportional-and-integral controller, V_c is the ac voltage in the ac-link capacitor, and the subscripts of d and q are the $d-q$ components, respectively. The dynamic model of the converter is represented in a $d-q$

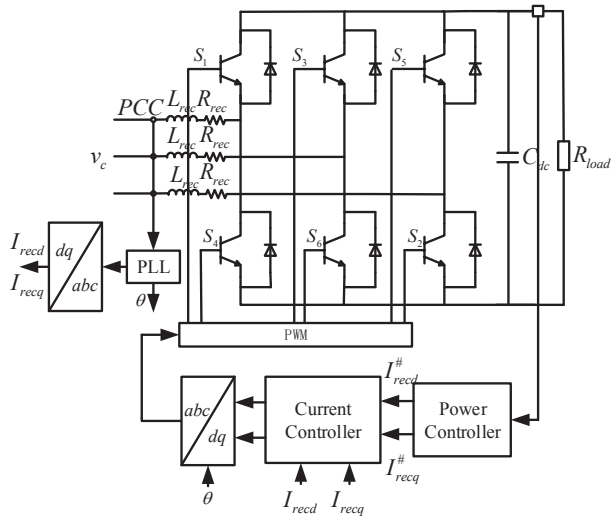

Fig. 3: Controller architecture of the constant power load

frame by the following state equations [20]:

$$V_{cd} = I_{recd}\left(R_{rec} + sL_{rec}\right) - \omega I_{recq} L_{rec} + D_d V_{dc}, \quad (2)$$

$$V_{cq} = I_{recq}\left(R_{rec} + sL_{rec}\right) + \omega I_{recd} L_{rec} + D_q V_{dc}, \quad (3)$$

$$sC_{dc}V_{dc} + I_{dc} = 1.5\left(D_d I_{recd} + D_q I_{recq}\right), \quad (4)$$

$$V_{dc} = I_{dc} Z_{load}, \quad (5)$$

where, I_{rec} is the input ac current. L_{rec} and R_{rec} represent the equivalent inductance and resistance of the L-filter installed on the input port of the converter, respectively. D is the duty ratio. V_{dc} and I_{dc} are the output dc voltage and current, respectively. C_{dc} is the dc capacitor. s is the Laplace operator. Z_{load} is the terminated load. It can be represented as $Z_{load} = f(V) = Z_i(V/V_0)^{\alpha_i}$, where α_i represents exponent coefficient, and Z_i represents voltage-resistance dependency. Nevertheless, since the output voltage of the tightly regulated power electronics converter is a constant value, Z_{load} is also a constant resistance in state-steady point. Furthermore, the classical PI-based voltage/current controllers ($G_v(s)$, $G_i(s)$) are embedded into (2)-(3) for dc voltage tracking and regulation. The steady-state value of the controlled signals is obtained:

$$I^*_{recd} = (V^*_{dc} - V_{dc})G_v(s), \quad (6)$$

$$I^*_{recq} = 0, \quad (7)$$

$$D_d V_{dc} = (I_{recd} - I^*_{recd})G_i(s) + V_{cd} + \omega L_{rec} I_{recq}, \quad (8)$$

$$D_q V_{dc} = (I_{recq} - I^*_{recq})G_i(s) + V_{cq} - \omega L_{rec} I_{recd}. \quad (9)$$

where, the superscript $*$ is the steady-state value. Using the small-signal perturbations on (1)-(3), the small-signal model of (2)-(3) are rewritten by (10)-(11).

$$\begin{aligned}\Delta V_{cd} = {} & \left(R_{rec} + sL_{rec}\right)\Delta I_{recd} - G_{PLL}(s) L_{rec} V^*_{cq} \Delta I_{recq} \\ & + D^*_d \Delta V_{dc} + \Delta D_d V^*_{dc} \\ & - G_{PLL}(s) L_{rec} \Delta V_{cq} I^*_{recq}, \end{aligned} \quad (10)$$

$$\begin{aligned}\Delta V_{cq} = {} & \left(R_{rec} + sL_{rec}\right)\Delta I_{recq} + G_{PLL}(s) L_{rec} V^*_{cq} \Delta I_{recd} \\ & + D^*_q \Delta V_{dc} + \Delta D_q V^*_{dc} \\ & + G_{PLL}(s) L_{rec} \Delta V_{cq} I^*_{recd}, \end{aligned} \quad (11)$$

To derive the input admittance matrix in a rotating reference frame, (10)-(11) can be written in matrix form:

$$\begin{aligned}\left[\mathbf{Y1}\right]_{\mathbf{2*2}} \begin{bmatrix} \Delta V_{cd} \\ \Delta V_{cq} \end{bmatrix} = {} & \left[\mathbf{Y2}\right]_{\mathbf{2*2}} \begin{bmatrix} \Delta I_{recd} \\ \Delta I_{recq} \end{bmatrix} + \left[\mathbf{Y4}\right]_{\mathbf{2*1}} \Delta V_{dc} \\ & + \left[\mathbf{Y3}\right]_{\mathbf{2*2}} \begin{bmatrix} \Delta D_d \\ \Delta D_q \end{bmatrix}, \end{aligned} \quad (12)$$

where

$$\left[\mathbf{Y1}\right]_{\mathbf{2*2}} = \begin{bmatrix} 1 & G_{PLL}(s) L_{rec} I^*_{recq} \\ 0 & 1 - G_{PLL}(s) L_{rec} I^*_{recd} \end{bmatrix},$$

$$\left[\mathbf{Y2}\right]_{\mathbf{2*2}} = \begin{bmatrix} R_{rec} + sL_{rec} & -G_{PLL}(s) L_{rec} V^*_{cq} \\ G_{PLL}(s) L_{rec} V^*_{cq} & R_{rec} + sL_{rec} \end{bmatrix},$$

$$\left[\mathbf{Y3}\right]_{\mathbf{2*2}} = \begin{bmatrix} V^*_{dc} & 0 \\ 0 & V^*_{dc} \end{bmatrix}, \left[\mathbf{Y4}\right]_{\mathbf{2*1}} = \begin{bmatrix} D^*_d \\ D^*_q \end{bmatrix}.$$

Applying the similar analysis, the small-signal model from (5) to (9) are written in matrix form:

$$\Delta V_{dc} = \left[\mathbf{Y5}\right]_{\mathbf{1*2}} \begin{bmatrix} \Delta I_{recd} \\ \Delta I_{recq} \end{bmatrix} + \left[\mathbf{Y6}\right]_{\mathbf{1*2}} \begin{bmatrix} \Delta D_d \\ \Delta D_q \end{bmatrix}, \quad (13)$$

$$\begin{aligned}\begin{bmatrix} \Delta D_d \\ \Delta D_q \end{bmatrix} = {} & \left[\mathbf{Y7}\right]_{\mathbf{2*2}} \begin{bmatrix} \Delta I_{recd} \\ \Delta I_{recq} \end{bmatrix} + \left[\mathbf{Y8}\right]_{\mathbf{2*2}} \begin{bmatrix} \Delta V_{cd} \\ \Delta V_{cq} \end{bmatrix} \\ & + \left[\mathbf{Y9}\right]_{\mathbf{2*1}} \Delta V_{dc}, \end{aligned} \quad (14)$$

where

$$\left[\mathbf{Y5}\right]_{\mathbf{1*2}} = \begin{bmatrix} \frac{1.5 D^*_d Z_{load}}{C_{dc} Z_{load} s + 1} & \frac{1.5 D^*_q Z_{load}}{C_{dc} Z_{load} s + 1} \end{bmatrix},$$

$$\left[\mathbf{Y6}\right]_{\mathbf{1*2}} = \begin{bmatrix} \frac{1.5 I^*_{recd} Z_{load}}{C_{dc} Z_{load} s + 1} & \frac{1.5 I^*_{recq} Z_{load}}{C_{dc} Z_{load} s + 1} \end{bmatrix},$$

$$\left[\mathbf{Y7}\right]_{\mathbf{2*2}} = \frac{1}{V^*_{dc}} \begin{bmatrix} G_i(s) & \omega^* L_{rec} \\ -\omega^* L_{rec} & G_i(s) \end{bmatrix},$$

$$\left[\mathbf{Y8}\right]_{\mathbf{2*2}} = \begin{bmatrix} \frac{1 - G_v(s) G_i(s)}{V^*_{dc}} & \frac{G_{PLL}(s) L_{rec} I^*_{recq}}{V^*_{dc}} \\ 0 & \frac{1 - G_{PLL}(s) L_{rec} I^*_{recd}}{V^*_{dc}} \end{bmatrix},$$

$$\left[\mathbf{Y9}\right]_{\mathbf{2*1}} = \frac{1}{V^*_{dc}} \begin{bmatrix} G_v(s) G_i(s) - D^*_d & -D^*_d \end{bmatrix}^T.$$

Substitute (13) into (12).

$$\begin{aligned}\left[\mathbf{Y1}\right]_{\mathbf{2*2}} \begin{bmatrix} \Delta V_{cd} \\ \Delta V_{cq} \end{bmatrix} = {} & \left(\left[\mathbf{Y2}\right]_{\mathbf{2*2}} + \left[\mathbf{Y4}\right]_{\mathbf{2*1}} \left[\mathbf{Y5}\right]_{\mathbf{1*2}}\right) \times \\ & \begin{bmatrix} \Delta I_{recd} \\ \Delta I_{recq} \end{bmatrix} + \left(\left[\mathbf{Y3}\right]_{\mathbf{2*2}} + \left[\mathbf{Y4}\right]_{\mathbf{2*1}} \left[\mathbf{Y6}\right]_{\mathbf{1*2}}\right) \begin{bmatrix} \Delta D_d \\ \Delta D_q \end{bmatrix}. \end{aligned} \quad (15)$$

Substitute (13) into (14).

$$\begin{aligned}\left(\left[\mathbf{1}\right]_{\mathbf{2*2}} - \left[\mathbf{Y9}\right]_{\mathbf{2*1}} \left[\mathbf{Y6}\right]_{\mathbf{1*2}}\right) \begin{bmatrix} \Delta D_d \\ \Delta D_q \end{bmatrix} = {} & \left[\mathbf{Y8}\right]_{\mathbf{2*2}} \\ \begin{bmatrix} \Delta V_{cd} \\ \Delta V_{cq} \end{bmatrix} + \left(\left[\mathbf{Y7}\right]_{\mathbf{2*2}} + \left[\mathbf{Y9}\right]_{\mathbf{2*1}} \left[\mathbf{Y5}\right]_{\mathbf{1*2}}\right) & \begin{bmatrix} \Delta I_{recd} \\ \Delta I_{recq} \end{bmatrix} \end{aligned} \quad (16)$$

Replace $\begin{bmatrix} \Delta D_d & \Delta D_q \end{bmatrix}^T$, and the input admittance matrix can be obtained as follows:

$$\begin{aligned}\mathbf{Y_{in}} = {} & \begin{bmatrix} Y_{dd} & Y_{dq} \\ Y_{qd} & Y_{qq} \end{bmatrix} = \\ & \left\{ \begin{array}{l} \left(\left[\mathbf{Y4}\right]\left[\mathbf{Y6}\right] + \left[\mathbf{Y3}\right]\right)\left(\left[\mathbf{1}\right] - \left[\mathbf{Y9}\right]\left[\mathbf{Y6}\right]\right)^{-1} \\ \left(\left[\mathbf{Y7}\right] + \left[\mathbf{Y9}\right]\left[\mathbf{Y5}\right]\right) + \left[\mathbf{Y4}\right]\left[\mathbf{Y5}\right] + \left[\mathbf{Y2}\right] \end{array} \right\}^{-1} \\ & \left\{ \begin{array}{l} \left[\mathbf{Y1}\right] - \left(\left[\mathbf{Y4}\right]\left[\mathbf{Y6}\right] + \left[\mathbf{Y3}\right]\right) \\ \left(\left[\mathbf{1}\right] - \left[\mathbf{Y9}\right]\left[\mathbf{Y6}\right]\right)^{-1}\left[\mathbf{Y8}\right] \end{array} \right\}. \end{aligned} \quad (17)$$

Therein, the PLL, voltage control loop, lines connecting between different CPLs and so on have been embedded in

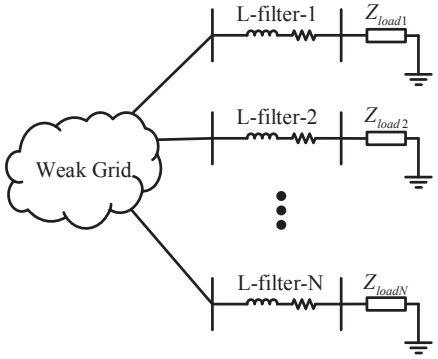

Fig. 4: Weak grid with N paralleled CPLs.

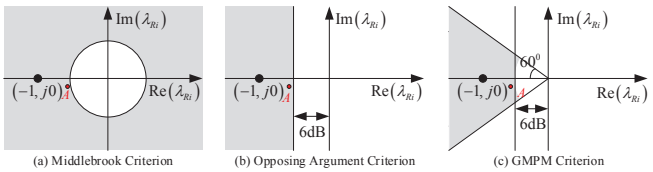

Fig. 5: The conventional stability forbidden region criteria.

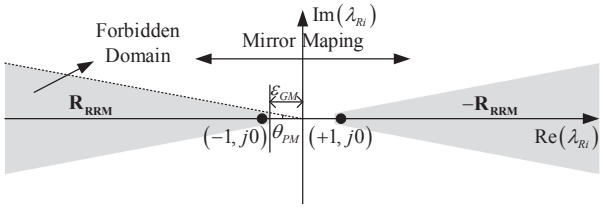

Fig. 6: Improved stability forbidden domain criterion.

the input admittance matrix. Their dynamics affect the input admittance matrix of the CPL, which further affect the stability domain of the cascaded system. As shown in Fig. 2, the output impedance matrix of the source subsystem consisting of line inductance and resistance, can be expressed as (18). In conclusion, the cascaded system return-ratio matrix can be presented as (19).

$$\mathbf{Z_{out}} = \begin{bmatrix} L_g s + R_g & -L_g\omega^* \\ L_g\omega^* & L_g s + R_g \end{bmatrix}. \tag{18}$$

$$\mathbf{R_{RRM}} = \mathbf{Z_{out}}\mathbf{Y_{in}}. \tag{19}$$

where R_g and L_g are severally the line resistance and inductance. $\mathbf{R_{RRM}}$ is the return-ratio matrix. Considering the weak grid incorporating multiple CPLs, which is shown in Fig. 4. The input admittance matrix of the i^{th} CPL obtained in (17), can be rewritten as $\mathbf{Y_{ini}}$. Thus, the whole input admittance matrix can be obtained through $\mathbf{Y_{in}} = \mathbf{Y_{in1}}//\mathbf{Y_{in2}}//...//\mathbf{Y_{inN}}$, and N represents the number of the CPLs.

III. Improved Stability Forbidden Criterion and Stability Domain Assessment Approach

According to the above-mentioned analysis, the cascaded system can be divided into two subsystem, *i.e.*, source subsystem and load subsystem. As shown in Fig. 1, $\mathbf{V_s}$, $\mathbf{i_s}$ and $\mathbf{Z_s}$ represent the voltage, current and impedance matrix of the source subsystem, respectively; $\mathbf{V_l}$, $\mathbf{i_l}$ and $\mathbf{Z_l}$ represent the voltage, current and impedance matrix of the load subsystem, respectively. Assume that the source subsystem is stable under an unload condition, *i.e.*, when the load is an open-circuit, and the load subsystem is stable when it is supplied by an ideal voltage source. The output voltage matrix of the connection bus is expressed [16].

$$\begin{aligned} \mathbf{V_p} &= \mathbf{Z_l}\mathbf{V_s}(\mathbf{Z_s}+\mathbf{Z_l})^{-1} + \mathbf{Z_s}\mathbf{V_l}(\mathbf{Z_s}+\mathbf{Z_l})^{-1} \\ &= \left(\mathbf{V_s} + \mathbf{Z_s}\mathbf{V_l}\mathbf{Z_l}^{-1}\right)\left(\mathbf{E} + \mathbf{Z_s}\mathbf{Z_l}^{-1}\right)^{-1}, \end{aligned} \tag{20}$$

where $\mathbf{E}$ is a unit matrix. Thus, the cascaded system is stable if and only if the $\left(\mathbf{E} + \mathbf{Z_s}\mathbf{Z_l}^{-1}\right)$ has no right pole. That is to say, the system is stable if and only if the net sum of anticlockwise encirclements of the point $(-1, j0)$ by the set of characteristic loci of the return-ratio matrix ($\mathbf{R_{RRM}}$) is equal to zero [15]. According to this concept, the system stability can be guaranteed by maintaining the characteristic values (λ_{Ri}, $i = 1, 2$) of $\mathbf{R_{RRM}}$ outside the certain forbidden domains. Meanwhile, the literature [15] said, "GNC is complex, and it is not suitable for the design of the AC system." For solving this issue, several forbidden region criteria have been proposed, such as Middlebrook Criterion, Gain and Phase Margin Criterion, and Opposing Argument Criterion [16], which are shown in Fig. 5. Meanwhile, as shown in the leftmost gray domain regarding Fig. 6, an improved stability forbidden criterion is proposed in (21)-(22).

$$|\arg(\lambda_{Ri})| \leq 180^0 - \theta_{PM}. \tag{21}$$

$$\mathrm{Re}(\lambda_{Ri}) \geq -\varepsilon_{GM}. \tag{22}$$

Through maintaining λ_{Ri} out of this forbidden domain, the small-signal stability can be guaranteed with phase margin (θ_{PM}) and gain margin (ε_{GM}). Therein, it is advisable that $\theta_{PM} = 60^0$ and $\varepsilon_{GM} = 0.5$ [19]. Furthermore, the conservatism of the proposed stability forbidden domain criterion can be further reduced through loosening θ_{PM} and ε_{GM}, i.e., $\theta_{PM} = 5^0$ and $\varepsilon_{GM} = 0.95$. Noting that the lower conservatism will be obtained if the stability forbidden domain is reduced. Compared with the area of the conventional forbidden criteria, the area of the proposed stability forbidden domain criterion is smallest. Thus, the proposed improved stability forbidden region criterion has lower conservatism. There is no doubt that the magnitude margin and phase margin in this paper, are chosen much less than other forbidden domain criterions. However, the aim of this paper is to obtain line inductance stability operation domain, which is advisable for power designers to obtain more accurate domain. Therefore, the magnitude margin and phase margin are chosen as minimum values. Additionally, the norm-based criteria is obtained through Middlebrook criterion, and the norm-based criteria has higher conservatism than Middlebrook criterion [15]. Consequently, the proposed stability forbidden domain criterion has lower conservatism among the previous simplified stability criteria. Furthermore, this proposed criterion is an indispensable preprocess for obtaining the line inductance stability operation domain through the guardian map theory, which is provided in Section III. The condition that guardian

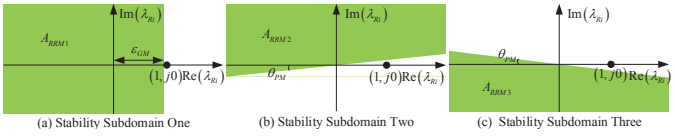

(a) Stability Subdomain One (b) Stability Subdomain Two (c) Stability Subdomain Three

Fig. 7: Decomposition of the stability operation domain.

map theory can be applied, is that the stability zone must be divided through several rectangles and trapezoids. Additionally, the cascaded system stability condition can be further switched to the condition that the characteristic loci of the $-\mathbf{R_{RRM}}$ does not encircle the point $(1, j0)$. Firstly, $\mathbf{R_{RRM}}$ and $-\mathbf{R_{RRM}}$ are separately rewritten as Jordan matrices, which are shown in (23) and (24)

$$\mathbf{R_{RRM}} = \mathbf{\Gamma^T} \begin{bmatrix} \lambda_{R1} & \wp \\ 0 & \lambda_{R2} \end{bmatrix} \mathbf{\Gamma}, \tag{23}$$

$$-\mathbf{R_{RRM}} = \mathbf{\Gamma^T} \begin{bmatrix} -\lambda_{R1} & \wp \\ 0 & -\lambda_{R2} \end{bmatrix} \mathbf{\Gamma}, \tag{24}$$

where $\mathbf{\Gamma}$ represents unitary matrix, and $\wp$ represents certain constant. If the characteristic loci of the $-\mathbf{R_{RRM}}$ does not encircle the point $(1, j0)$, (25) can be satisfied, which can be switched to (26) further

$$\det\left(-\mathbf{R_{RRM}} - \mathbf{E}\right) \neq 0, \text{ for all } s = j\omega. \tag{25}$$

$$\begin{aligned} &\det\left(\mathbf{\Gamma}^T \begin{bmatrix} -\lambda_{R1} & \wp \\ 0 & -\lambda_{R2} \end{bmatrix} \mathbf{\Gamma} - \mathbf{\Gamma}^T \begin{bmatrix} 1 & 0 \\ 0 & 1 \end{bmatrix} \mathbf{\Gamma}\right) \neq 0 \\ &\Rightarrow \det\left(\mathbf{\Gamma}^T \begin{bmatrix} -\left(\lambda_{R1}+1\right) & \wp \\ 0 & -\left(\lambda_{R2}+1\right) \end{bmatrix} \mathbf{\Gamma}\right) \neq 0 \\ &\Rightarrow \det\left(\begin{bmatrix} -\left(\lambda_{R1}+1\right) & \wp \\ 0 & -\left(\lambda_{R2}+1\right) \end{bmatrix}\right) \neq 0 \\ &\Rightarrow \left(\lambda_{R1}+1\right)\left(\lambda_{R2}+1\right) \neq 0. \end{aligned} \tag{26}$$

where $\omega = 2\pi f$. Secondly, the similar result is obtained that the characteristic loci of $\mathbf{R_{RRM}}$ does not encircle the point $(-1, j0)$.

$$\begin{aligned} &\det\left(\mathbf{R_{RRM}} + \mathbf{E}\right) \text{ for all } s = j\omega \\ &= \det\left(\mathbf{\Gamma}^T \begin{bmatrix} \lambda_{R1} & \wp \\ 0 & \lambda_{R2} \end{bmatrix} \mathbf{\Gamma} + \mathbf{\Gamma}^T \begin{bmatrix} 1 & 0 \\ 0 & 1 \end{bmatrix} \mathbf{\Gamma}\right) \\ &= \det\left(\mathbf{\Gamma}^T \begin{bmatrix} \lambda_{R1}+1 & \wp \\ 0 & \lambda_{R2}+1 \end{bmatrix} \mathbf{\Gamma}\right) \\ &= \det\left(\begin{bmatrix} \lambda_{R1}+1 & \wp \\ 0 & \lambda_{R2}+1 \end{bmatrix}\right) \\ &= \left(\lambda_{R1}+1\right)\left(\lambda_{R2}+1\right) \neq 0. \end{aligned} \tag{27}$$

Furthermore, the small-signal stability domain can be obtained through $-\mathbf{R_{RRM}}$. Small-signal stability domain consists of the sum aggregate of the three subregions, *e.g.*, A_{RRM1}, A_{RRM2} and A_{RRM3}. Therein, A_{RRM1} is obtained by translation mapping. A_{RRM2} and A_{RRM3} are obtained by rotation mapping, which are green domains shown in Fig. 7. Meanwhile, these subregions can be given by (28)-(30), where, $\mathbf{R_{ARRM1}}$, $\mathbf{R_{ARRM2}}$ and $\mathbf{R_{ARRM3}}$, which are defined as intermediate matrices, are Hurwitz. In engineering and stability theory, a square matrix $\mathbf{R}$ is called a Hurwitz matrix if every characteristic value of $\mathbf{R}$ has strictly negative real part, that is $\mathrm{Re}\left[\lambda_i\right] < 0$ for each characteristic value λ_i.

$$A_{RRM1}: \quad \mathbf{R_{ARRM1}} = -\mathbf{R_{RRM}} - \varepsilon_{\mathbf{GM}}\mathbf{E}. \tag{28}$$

$$A_{RRM2}: \quad \mathbf{R_{ARRM2}} = -\mathbf{R_{RRM}} \times \mathbf{e}^{\mathbf{j}\theta_{\mathbf{PM}}}. \tag{29}$$

$$A_{RRM3}: \quad \mathbf{R_{ARRM3}} = -\mathbf{R_{RRM}} \times \mathbf{e}^{-\mathbf{j}\theta_{\mathbf{PM}}}. \tag{30}$$

The weak grid is one complex system with numerous distributed resources, energy storages and loads. In order to depict this complex system stability, the short circuit ratio ($SCR \approx 1/L_g$) is widely applied, and the weak grid is emulated by the utility grid in series with a line impedance [3]. Therefore, as the structure of the weak grid changes, such as renewable energy fluctuation, load fluctuation and so on, the equivalent line output impedance will be always changed. Thus, the conventional impedance-based stability operation point identification need to be expanded into stability operation domain identification considering the equivalent line impedance fluctuation. Likewise, the proposed stability operation domain identification method can also be regarded as the robust stability identification method regarding line impedance, which provides the guidance for power system planning and stabilization method researches. For offline design or online tuning, power system engineers prefer to obtain stability domain rather than one or several stability operation points to facilitate their multi parameter regulation in weak grids. When power system engineers design the structure regarding weak grids, the equivalent line impedance can be extended from one single stability point to a certain stability range. To sum up, the conventional impedance-based stability assessment should be expanded. Therein, the cascaded system return-ratio matrix under line inductance fluctuation can be shown as follows:

$$\begin{aligned} &\mathbf{R_{RRM}} = \mathbf{Z_{out}}\mathbf{Y_{in}} \\ &= \begin{bmatrix} \left(L_{g0}+\Delta L_g\right)s + R_g & -\left(L_{g0}+\Delta L_g\right)\omega^* \\ \left(L_{g0}+\Delta L_g\right)\omega^* & \left(L_{g0}+\Delta L_g\right)s + R_g \end{bmatrix} \mathbf{Y_{in}} \\ &= \begin{bmatrix} L_{g0}s + R_g & -L_{g0}\omega^* \\ L_{g0}\omega^* & L_{g0}s + R_g \end{bmatrix} \mathbf{Y_{in}} \\ &+\Delta L_g \begin{bmatrix} s & -\omega^* \\ \omega^* & s \end{bmatrix} \mathbf{Y_{in}} \\ &= \mathbf{Z_{out0}}\mathbf{Y_{in}} + \Delta L_g \mathbf{\Delta Z_{out}}\mathbf{Y_{in}} \end{aligned} \tag{31}$$

where L_{g0} and ΔL_g represent the original line inductance and line inductance variation value, respectively. Define $\mathbf{R_{RRM0}} = \mathbf{Z_{out0}}\mathbf{Y_{in}}$, $\mathbf{R_{RRMz}} = \mathbf{\Delta Z_{out}}\mathbf{Y_{in}}$ and $\rho = \Delta L_g$. $\mathbf{R_{RRM0}}$ represents return-ratio matrix in stable operation point, and $\mathbf{R_{RRMz}}$ represents return-ratio variation matrix. ρ represents line inductance variation parameter. Therein, when system is stable, the maximum change range regarding ρ should be obtained. Based on this, the stability domain assessment approach is proposed by the guardian map theory. According to the foresaid analysis, the cascaded system is stable if one of the intermediate matrices is Hurwitz. Thus, the line inductance stability operation domain is switched to the condition that intermediate matrix is Hurwitz. In order to simplify variables, the intermediate matrix is redefined as $\mathbf{I}$. Moreover, the intermediate matrix ($\mathbf{I} = \mathbf{R_{ARRM1}}$, $\mathbf{R_{ARRM2}}$

or $\mathbf{R_{ARRM3}}$) can be expressed:

$$\mathbf{I} = \mathbf{I_0} + \rho \mathbf{I_z}, \tag{32}$$

where $\mathbf{I_0}$ represents intermediate matrix in stable operation point, and $\mathbf{I_z}$ represents intermediate line inductance variation matrix. In light of (31), the variation of line inductance is linearly related to the intermediate matrix. Therefore, it is convenient to obtain (32). For example, when $\mathbf{I} = \mathbf{R_{ARRM1}}$, the following equation can be obtained

$$\begin{aligned} &\mathbf{I} = -\mathbf{R_{RRM}} - \varepsilon_{\mathbf{GM}}\mathbf{E} \\ &= -\left(\mathbf{Z_{out0}Y_{in}} + \Delta L_g \mathbf{\Delta Z_{out} Y_{in}}\right) - \varepsilon_{\mathbf{GM}}\mathbf{E} \\ &= \left(-\mathbf{Z_{out0}Y_{in}} - \varepsilon_{\mathbf{GM}}\mathbf{E}\right) + \Delta L_g \left(-\mathbf{\Delta Z_{out} Y_{in}}\right) \end{aligned} \tag{33}$$

where $\left(-\mathbf{Z_{out0}Y_{in}} - \varepsilon_{\mathbf{GM}}\mathbf{E}\right) = \mathbf{I_0}$, $\left(-\mathbf{\Delta Z_{out} Y_{in}}\right) = \mathbf{I_z}$ and $\Delta L_g = \rho$. In order to obtain the line inductance stability operation domain, several definitions are provided in advance [21].

Definition 1: Assume that $\mathbf{D} \subseteq \mathbf{R^{n\times n}}$ represents one open set. The map $f : \mathbf{R^{n\times n}} \to \mathbf{R}$ is regarded to defend the set $\mathbf{D}$ if $f(\mathbf{I}) \neq \mathbf{0}$ for all $\mathbf{I} \in \mathbf{D}$, and $f(\mathbf{I}) = \mathbf{0}$ for all $\mathbf{I} \in \partial\mathbf{D}$ ($\partial\mathbf{D}$ represents the boundary of the set $\mathbf{D}$). This map f is named a guardian map for $\mathbf{D}$.

Definition 2: Give one matrix, $\mathbf{I} \subseteq \mathbf{R^{n\times n}}$, assume that $\bar{\lambda}_i(\mathbf{I})$, $i = 1, 2, ..., k$, represent the real parts of the non-zero characteristic values of $\mathbf{I}$, and $r_0 = -\infty$, $r_{k+1} = +\infty$, and $r_i = -1/\bar{\lambda}_i(\mathbf{I})$. Further the order set $\Theta(\mathbf{I}) = \{r_0, r_1, ..., r_{k+1}\}$, thereinto, $r_i < r_{i+1}$.

Definition 3: Assume that $\mathbf{I_1} \in \mathbf{R^{n\times n}}$ and $\mathbf{I_2} \in \mathbf{R^{m\times m}}$. Meanwhile, mspec($\mathbf{I_1} \bigodot \mathbf{I_2}$)=mspec($\bar{\mathbf{I}}$)=$\{\lambda_i(I) + \lambda_j(I), i = 2, 3, ..., n$ and $j = 1, 2, ..., i-1\}$, where $\bigodot$ represents Bialternate product, and mspec represents multispectrum of matrix $\mathbf{I} \in \mathbf{R}^{n\times n}$, *i.e.*, the set consisting of all eigenvalues of $\mathbf{I}$, including repeated eigenvalues.

Lemma 1 [21]: For one open interval $\Omega \in R$ and $\mathbf{I_0}, \mathbf{I_z} \in \mathbf{R^{n\times n}}$, define $\bar{\mathbf{I}}_0 \triangleq 2\mathbf{I_0} \odot \mathbf{E}$ and $\bar{\mathbf{I}}_z \triangleq 2\mathbf{I_z} \odot \mathbf{E}$. Therefore, for all $\rho \in \Omega$ and $0 \in \Omega$, $\mathbf{I} = \mathbf{I_0} + \rho\mathbf{I_z}$ is Hurwitz if and only if $\mathbf{I_0}$ is a Hurwitz matrix and $0 \in \Omega \in \Theta(\mathbf{I_0}^{-1}\mathbf{I_z}) \cap \mathbf{\Theta}(\bar{\mathbf{I}}_\mathbf{0}^{-1}\bar{\mathbf{I}}_\mathbf{z})$.

According to (31), the return-ratio matrix of cascaded system is a function regarding frequency. Once the system frequency is determined, the return-ratio matrix can be considered as an inductance-dependent linear time-invariant matrix. Furthermore, the set of correlated frequencies affecting the system stability is chosen as $f_{tab} = [1, 2, ..., 20000]$ Hz. Meanwhile, the steps for calculating the stability domain of line inductance are shown in *Solving Process*.

Applying same solving process, the stability domain of the cascaded system (U_2, U_3) can be provided, which are through $\mathbf{R_{ARRM2}}$ and $\mathbf{R_{ARRM3}}$. Consequently, the line inductance stability domain is $U = U_1 \cup U_2 \cup U_3$. Although Kronecker sum is always utilized to construct guardian map, Bialternate product has lower computational complexity [7], [21]. Therein, the dimensions of guardian map matrix constructed by Kronecker sum and Bialternate product are $n^2 \times n^2$ and $0.5n(n-1) \times 0.5n(n-1)$, respectively. Thus, this paper uses Bialternate product to construct guardian map. In this paper, the set of correlated frequencies is chosen as $f_{tab} = [1, 2, ..., 20000]Hz$. In each iteration, the frequency is set as one value. In theory, when the frequency is set,

Algorithm 1 *Solving Process*

Initialization: U_1 is full set; $f = f_1$; $\mathbf{I} = \mathbf{R_{ARRM1}}$.
Iteration: ($i \leq p$)

1: Form $\mathbf{I_0}$ and $\mathbf{I_z}$ when $f = f_i$;
2: Obtain the characteristic values of $\bar{\mathbf{I}}_\mathbf{0}$, $\bar{\mathbf{I}}_\mathbf{z}$ and $\bar{\mathbf{I}}_\mathbf{0}^{-1}\bar{\mathbf{I}}_\mathbf{z}$;
3: Construct $\Theta(\mathbf{I}) = \{\mathbf{r_0}, \mathbf{r_1}, ..., \mathbf{r_{k+1}}\}$ in light of Definition 2;
4: Judge if $\mathbf{I}$ is Hurwitz for $\rho_i \in (r_i, r_{i+1})$. If OK, the system stability is ensured in the open set;
5: Solve the union of all open sets where the system stability is ensured, and obtain line inductance stability domain U_{1i};
6: Obtain the intersection of all stability domain, *e.g.*, $U_1 = U_1 \cap U_{1i}$;
7: $i = i + 1$;

TABLE I: The cascaded system parameters

Parameters	Values	Parameters	Values
$G_{PLL}(s)$	$k_{pp} = 0.58, k_{pi} = 10$	C_{dc}	$20mF$
$G_v(s)$	$k_{vp} = 2, k_{vi} = 10$	V_{dc}^*	$600V$
$G_i(s)$	$k_{ip} = 0.4, k_{ii} = 30$	ω^*	100π
L_{rec}	$1mH$	R_{rec}	$0.1m\Omega$
R_g	0.5Ω	I_{rec}^*	$60A$
ε_{GM}	0.95	θ_{PM}	5^0

the capacitive line impedance can be regarded as one pure resistor and one pure capacitor, which can be further regarded as one pure resistor and one specific negative inductor. Since this negative inductor does not change relative derivation and Solving Process, the proposed stability criterion is still applicable for capacitive line impedance.

IV. Simulation Results

The conservatism of the improved stability forbidden domain criterion and the effectiveness of the proposed line inductance stability domain assessment approach for weak grids with multiple CPLs are severally verified through MATLAB/Simulink in one computing with intel(R) Core(TM) i5-4590 CPU @ 3.30 GHz and 4 GB of RAM. Thereinto, the system topology is depicted in Fig. 4. In this system, the CPL is stable when supplied by an ideal voltage source, and main-grid is stable when unload, *i.e.*, when the load is an open-circuit. Meanwhile, the system parameters are provided in Table I.

A. Conservatism

In order to better compare with the previous literatures, the number of the CPLs is chosen as one, which is same to the structure in [15]. At initial time, the line inductance is $L_g = 0.6$mH. Firstly, $\mathbf{I_0}$ regarding $\mathbf{R_{ARRM1}}$ does not have positive real characteristic values when the frequency is changed from 0 to 20000 Hz, and the maximum real part of characteristic value is -0.4651. Thus, the intermediate matrix $\mathbf{R_{ARRM1}}$ is Hurwitz, and the cascaded system must be stable. Secondly, since the singular-value criterion has the minimum conservatism among four norm-based criteria [15]. Thus, the

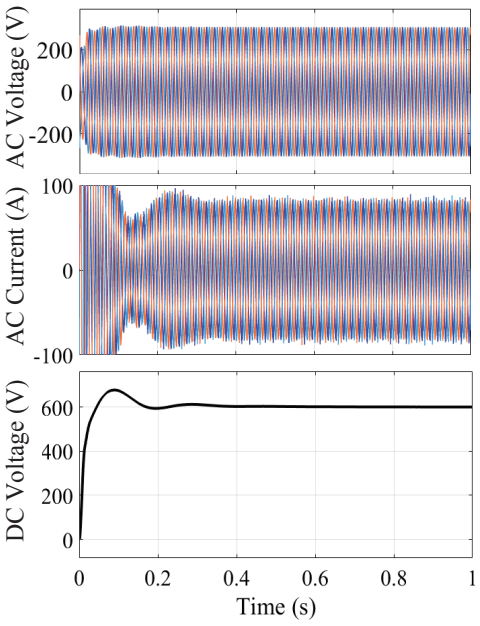

Fig. 8: The three-phase ac voltage/current and dc voltage waveforms in initial system state.

conservatism comparison between the proposed criterion and singular-value criterion is provided. Therein, when the system frequency is set as $32Hz$, the output impedance matrix, input admittance matrix and return-ratio matrix are shown as follows:

$$\mathbf{Z_{out}} = \begin{bmatrix} -0.1884 & 0.5 + j0.1206 \\ -0.5 - j0.1206 & -0.1884 \end{bmatrix}, \quad (34)$$

$$\mathbf{Y_{in}} = \begin{bmatrix} 2.5402 - j0.0582 & 0.0138 + j0.0715 \\ -0.0653 - j0.2726 & -0.0252 - j0.028 \end{bmatrix}, \quad (35)$$

$$\mathbf{R_{RRM}} = \begin{bmatrix} -0.4783 - j0.1332 & 0.0118 + j0.0305 \\ -1.2648 - j0.2258 & -0.0065 - j0.0322 \end{bmatrix}. \quad (36)$$

Under this case, $\bar{\sigma}\left(\mathbf{Z_{out}}\right) = 0.5878$, $\bar{\sigma}\left(\mathbf{Y_{in}}\right) = 2.5481$ and $\bar{\sigma}\left(\mathbf{Z_{out}}\right)\bar{\sigma}\left(\mathbf{Y_{in}}\right) = 1.4978$. The relative illustrations can be found in the literature [15]. Therefore, the value of the singular-value criterion is larger than one when the frequency is set as $32Hz$. Consequently, the cascaded system may be unstable. Furthermore, the two characteristic values of the return-ratio matrix are severally $-0.5154 - j0.2003$ and $0.0436 - j0.035$. Therein, the leftmost characteristic root is depicted as point A in Fig. 5. As a result, the cascaded system may be unstable. Furthermore, the conservatism can be compared through real simulation time-domain waveforms. As shown in Fig. 8, the cascaded system is stable, which illustrates that the conservatism of the proposed improved stability criterion is lower than that of the two series simplified criteria.

B. Effectiveness

Firstly, the number of the CPLs is chosen as one, and the simulation parameters are given in Table I. In this case,

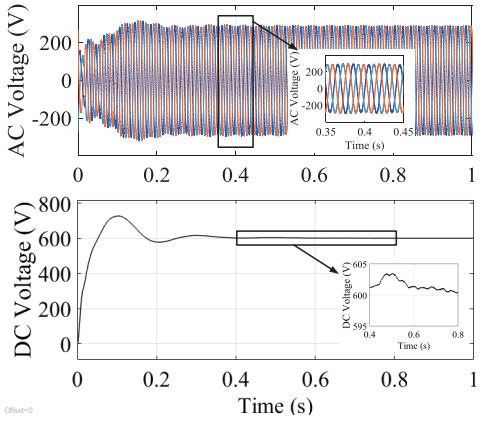

Fig. 9: The three-phase ac voltage under $L_g = 1.319mH$.

the clear line inductance range of stable domain is $L_g = [0, 1.319]\,\mathrm{mH}$, which is obtained through the point-by-point simulation approach. Noting that the point-by-point simulation approach is able to provide stability domain boundary through the numerical simulation. Although this approach is relatively accurate, it is too slow in calculation speed. Especially when numerous CPLs are embedded in the system. As shown in Fig. 9, the mild low-frequency oscillation has occurred in this system. Moreover, the generalized Nyquist curve of the return-ratio matrix is shown in Fig. 10(b). Since the stability of cascaded system increases with the decrease of line inductance, this paper only chooses the domain where the line inductance increases. According to the proposed solving process, the line inductance stability domain is $L_g = [0, 1.228]\,\mathrm{mH}$. Meanwhile, if the ε_{GM}=0.99, the line inductance stability domain is extended as $L_g = [0, 1.285]\,\mathrm{mH}$. Thus, if ε_{GM} squints towards 1 and θ_{PM} squints towards 0^0, the proposed criterion will become approximately one necessary and sufficient condition.

First and foremost, the line inductance of the weak grid is selected that $L_g = 0.5\mathrm{mH}$. Under this case, the cascaded system must be stable. The same result can be obtained through observing the generalized Nyquist curve in Fig. 10(a). Evidently, as shown in Fig. 11, the input ac voltage and output dc voltage waveforms of the converter are stable. Thus, the performance of the proposed stability domain approach is guaranteed. Furthermore, the line inductance is changed from $L_g = 0.5\mathrm{mH}$ to $L_g = 2.6\mathrm{mH}$, the line inductance is outside stability domain. As a result, the cascaded system may be unstable, and this conclusion is verified through the generalized Nyquist curve in Fig. 10(c). Furthermore, as shown in Fig. 12, low-frequency oscillation has occurred in the cascaded system. In order to further verify the performance of the proposed approach, the line inductance is further changed to $L_g = 4\mathrm{mH}$. The line inductance of the cascaded system is far away from the line inductance stability domain, and the system stability is likely to be destroyed. Therein, this conclusion is also verified through the generalized Nyquist curve in Fig. 10(d). As shown in Fig. 13, the instability phenomenon has occurred in the cascaded system. Therein,

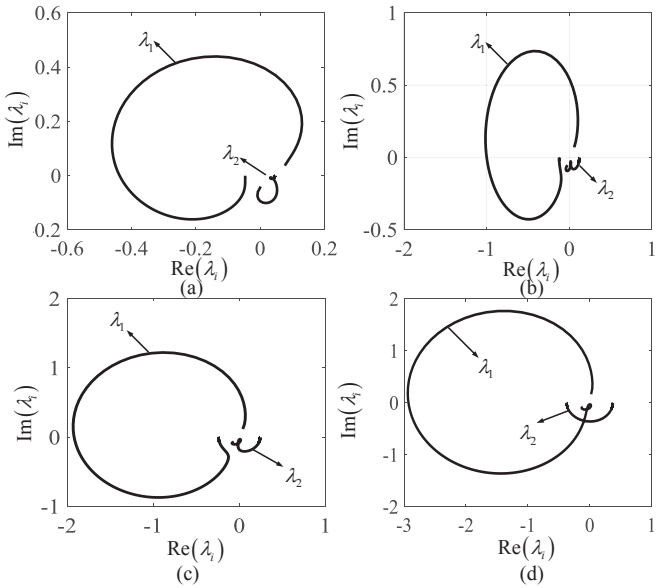

Fig. 10: The generalized Nyquist curve: (a) under $L_g = 0.5\text{mH}$; (b) under $L_g = 1.319\text{mH}$; (c) under $L_g = 2.6\text{mH}$; (d) under $L_g = 4\text{mH}$

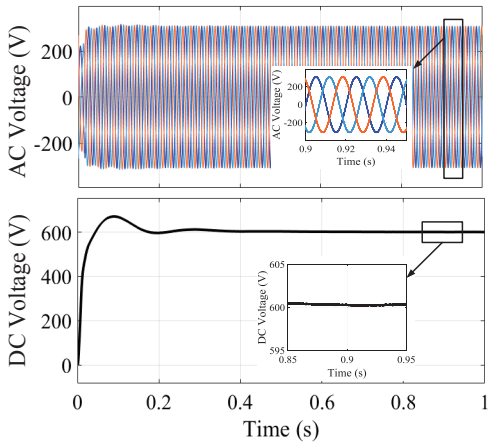

Fig. 11: The three-phase ac voltage and dc voltage waveforms under $L_g = 0.5\text{mH}$.

the ac voltage waveform is divergent and unstable. Meanwhile, the output dc voltage of the converter is unstable. In summary, the simulation results show that the proposed stability domain approach is effective.

Furthermore, the PLL and the voltage control loop dynamics will affect the input admittance matrix of the CPL, which further affect the stability operation domain of the cascaded system. In order to verify these impacts, the stability domains under different control parameters have been provided in Table II.

Secondly, the number of CPLs is chosen as three, and the terminated loads of these CPLs are severally chosen as 30Ω, 20Ω and 20Ω. Under this case, the line inductance stability domain of the cascaded system is $L_g = [0, 0.5846]\,\text{mH}$. As the number of CPLs increases, the system stability domain is reduced. At the beginning, the line inductance of the cascaded

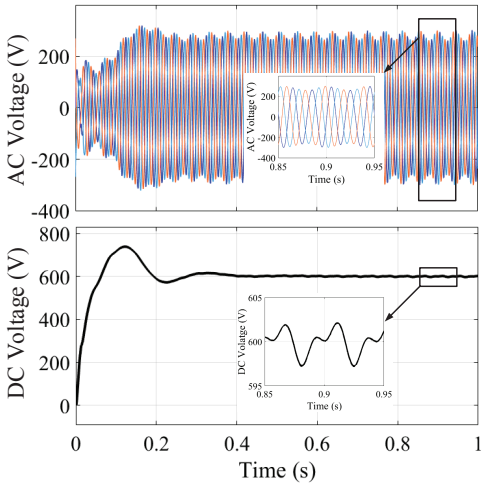

Fig. 12: The three-phase ac voltage and dc voltage waveforms under $L_g = 2.6\text{mH}$.

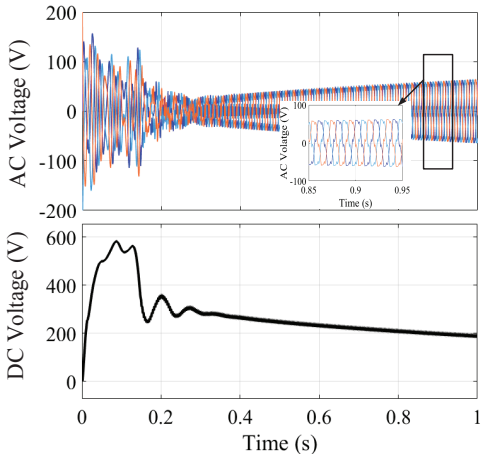

Fig. 13: The three-phase ac voltage and dc voltage waveforms under $L_g = 4\text{mH}$.

system is chosen as $L_g = 0.35\text{mH}$. Since the line inductance is located in stability domain, the cascaded system must be stable. As depicted in Fig. 14, both voltage and current waveforms are stable. Furthermore, the line inductance is changed from $L_g = 0.35\text{mH}$ to $L_g = 0.58\text{mH}$, which is closed to stability operation boundary. As shown in Fig. 15, both voltage and current waveforms are still stable. The line inductance is further set as $L_g = 0.6\text{mH}$, which represents the line inductance lies outside the stability domain. Under this case, the mild low-frequency oscillation has occurred in this

TABLE II: The stability operation domains under the different controller parameters

PLL Controller	Stability Domain	Voltage Controller	Stability Domain
$0.78 + 10/s$	$[0, 1.198]$ mH	$3 + 10/s$	$[0, 0.766]$ mH
$0.435 + 10/s$	$[0, 1.248]$ mH	$1.5 + 10/s$	$[0, 1.697]$ mH
$0.58 + 15/s$	$[0, 1.227]$ mH	$2 + 15/s$	$[0, 1.216]$ mH
$0.58 + 7.5/s$	$[0, 1.228]$ mH	$2 + 7.5/s$	$[0, 1.231]$ mH

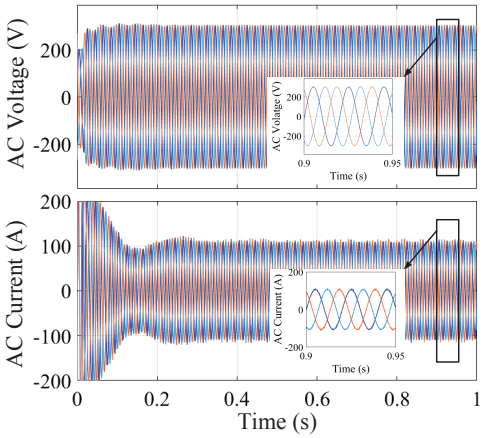

Fig. 14: The three-phase ac voltage/current waveform under $L_g = 0.35\text{mH}$.

system, which is shown in Fig. 16. In order to further verify the performance of the proposed approach, the line inductance is further changed to $L_g = 1\text{mH}$. The line inductance of the cascaded system is far away from the line inductance stability domain, and the system stability is likely to be destroyed. As shown in Fig. 17, the instability phenomenon has occurred in the cascaded system. Therein, the ac voltage waveform is divergent and unstable. To sum up, the effectiveness of the proposed approach for weak grids with multiple CPLs case is verified. Additionally, the computation time of the proposed line inductance stability operation domain identification method with one CPL and three CPLs are 2.016s and 2.023s, respectively. Furthermore, the dynamics of lines connecting between different CPLs will affect the input admittance matrix of the CPL, which further affect the stability operation domain of the cascaded system. In order to verify these impacts, the L-filter of the second CPL is changed from $L_{rec2} = 1mH$ and $R_{rec2} = 0.1m\Omega$ to $L_{rec2} = 1.3mH$ and $R_{rec2} = 0.1m\Omega$. Under this case, the line inductance stability domain of the cascaded system is $L_g = [0, 0.4937]\, mH$. Thus, the line inductance stability operation domain with low computation burden is obtained through the proposed method in this paper.

V. Experimental Results

The effectiveness of the proposed line inductance stability domain assessment approach for three phase weak grids with CPLs is verified by experiment, whose topology is shown in Fig. 2. The control systems of the converter are implemented in a TMS320F28335DSP+XC6SLX9FPGA system with the switch frequency of 19.2kHz and furthermore, RS232&RS485 is applied for the digital control system communication circuit, and HNV025A and HNC-100LA are separately utilized for the voltage and current measurements. The TELEDYNE LECROY Oscilloscope is utilized to show the experimental waveforms. The detailed section can be found in our previous literature [22]. The output voltage of the tightly regulated converter is reduced to 60V, and the terminated load is set as 10Ω. Therefore, the power rating of the resistance is $0.36kW$.

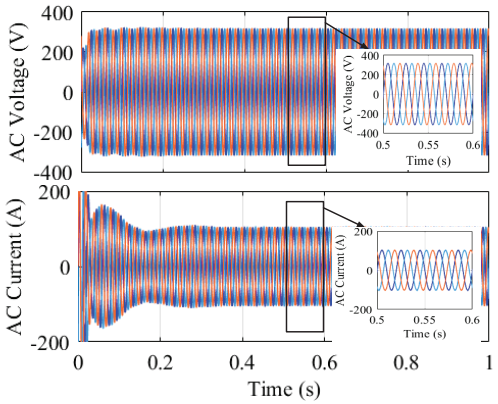

Fig. 15: The three-phase ac voltage/current waveform under $L_g = 0.58\text{mH}$.

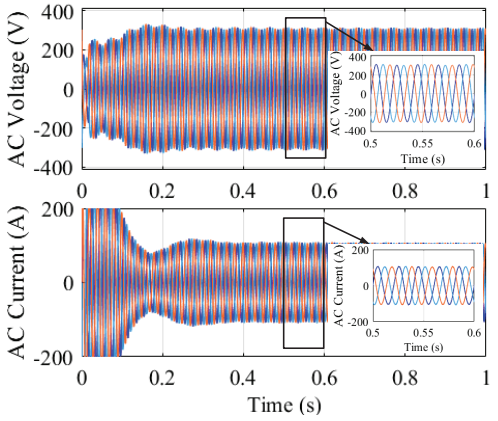

Fig. 16: The three-phase ac voltage/current waveform under $L_g = 0.6\text{mH}$.

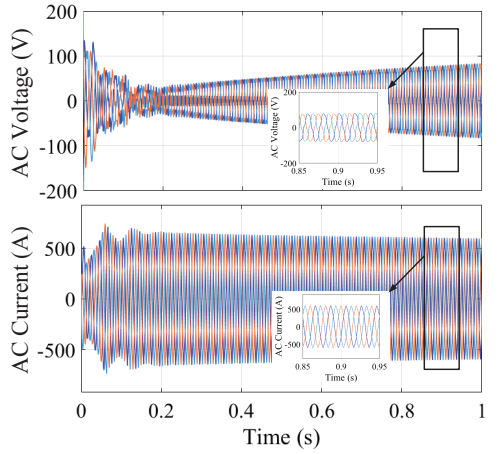

Fig. 17: The three-phase ac voltage/current waveform under $L_g = 1\text{mH}$.

Meanwhile, the system other parameters are shown in Table I.

Under this case, the line inductance stability domain of the cascaded system is calculated as $L_g = [0, 1.251]\,\text{mH}$. First and

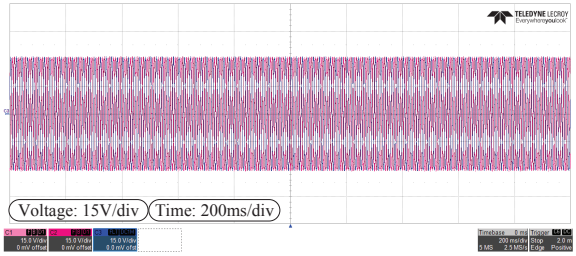

Fig. 18: The three-phase voltage experimental waveform under $L_g = 0.5\text{mH}$.

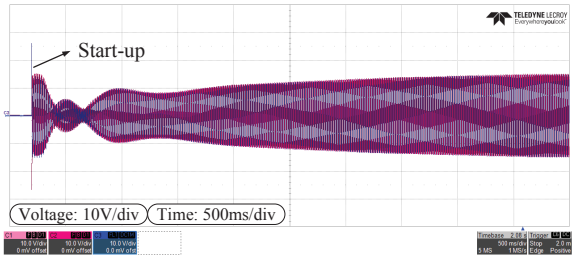

Fig. 19: The three-phase voltage experimental waveform under $L_g = 2.6\text{mH}$.

foremost, the line inductance is also $L_g = 0.5\text{mH}$. Therefore, the cascaded system must be stable. Sufficiently obvious, as shown in Fig. 19, the measured output ac voltage waveform of the converter is stable. Thus, the effectiveness of the proposed approach can be guaranteed. Furthermore, the line inductance is changed from $L_g = 0.5\text{mH}$ to $L_g = 2.6\text{mH}$. Since line inductance is outside the line inductance stability domain, the experimental system may be unstable, and the stability of the cascaded system can be clearly verified by checking the time-domain experimental waveforms. As seen in Fig. 20, the instability phenomenon has occurred in the cascaded system. The experimental results show that the proposed approach is effective to assess the line inductance stability domain.

VI. Conclusion

For rural areas, the main grid has been usually not an ideal voltage source but a weak grid where it contains inductive impedance, which results in low frequency oscillation and harmonic oscillation phenomena, and CPLs would further exacerbate these phenomena. Meanwhile, since the play and plug characteristic of modern power system, the line inductance often changes. Therefore, this paper has proposed a stability-oriented line inductance stability domain assessment approach for weak grids with CPLs. Firstly, this paper has built the source impedance matrix and load admittance matrix. Moreover, an improved stability forbidden domain criterion has been constituted through related mapping transformation process. Compared with two previous improved stability criteria, the conservatism of the proposed criterion has been reduced. Likewise, the line inductance stability domain has been obtained through defined three intermediate matrices and guardian map theory. Finally, the simulation and experiment results have been provided to verify the conservatism and efficiency of the proposed stability domain approach.

References

[1] W. Rui, S. Qiuye, Z. Pinjia, G. Yonghao, Q. Dehao and W. Peng, "Reduced-Order Transfer Function Model of the Droop-Controlled Inverter via Jordan Continued-Fraction Expansion," *IEEE Trans. Energy Convers.*, vol. 35, no. 3, pp. 1585-1595, Sept. 2020.

[2] R. Wang, Q. Sun, D. Ma and Z. Liu, "The Small-Signal Stability Analysis of the Droop-Controlled Converter in Electromagnetic Timescale," *IEEE Trans. Sustain. Energy*, vol. 10, no. 3, pp. 1459-1469, July 2019.

[3] W. Wu et al., "Sequence Impedance Modeling and Stability Comparative Analysis of Voltage-Controlled VSGs and Current-Controlled VSGs," *IEEE Trans. Ind. Electron.*, vol. 66, no. 8, pp. 6460-6472, Aug. 2019.

[4] B. Fan, S. Guo, J. Peng, Q. Yang, W. Liu and L. Liu, "A Consensus-Based Algorithm for Power Sharing and Voltage Regulation in DC Microgrids," *IEEE Trans. Ind. Informat.*, vol. 16, no. 6, pp. 3987-3996, June 2020.

[5] Z. Li and M. Shahidehpour, "Small-Signal Modeling and Stability Analysis of Hybrid AC/DC Microgrids," *IEEE Trans. Smart Grid*, vol. 10, no. 2, pp. 2080-2095, March 2019.

[6] L. Huang et al., "Grid-Synchronization Stability Analysis and Loop Shaping for PLL-based Power Converters With Different Reactive Power Control," *IEEE Trans. Smart Grid.*, to be published, doi: 10.1109/TSG.2019.2924295.

[7] W. Rui, S. Qiuye, M. Dazhong and H. Xuguang, "Line Impedance Cooperative Stability Region Identification Method for Grid-Tied Inverters Under Weak Grids," *IEEE Trans. Smart Grid*, vol. 11, no. 4, pp. 2856-2866, July 2020.

[8] R. D. Middlebrook, "Input filter considerations in design and application of switching regulators," *Proc. IEEE Ind. Appl. Soc. Annu. Meeting*, 1976.

[9] J. M. Undrill and T. E. Kostyniak, "Subsynchronous oscillations part 1 comprehensive system stability analysis," *IEEE Trans. Power Appar. Syst.*, vol. 95, no. 4, pp. 1446-1455, July 1976.

[10] F. Liu, J. Liu, H. Zhang and D. Xue, "Stability Issues of $Z + Z$ Type Cascade System in Hybrid Energy Storage System (HESS)," *IEEE Trans. Power Electron.*, vol. 29, no. 11, pp. 5846-5859, Nov. 2014.

[11] A. Rygg and M. Molinas, "Apparent Impedance Analysis: A Small-Signal Method for Stability Analysis of Power Electronic-Based Systems," *IEEE J. Emerg. Sel. Topics Power Electron.*, vol. 5, no. 4, pp. 1474-1486, Dec. 2017.

[12] J. Lyu, X. Zhang, X. Cai and M. Molinas, "Harmonic State-Space Based Small-Signal Impedance Modeling of a Modular Multilevel Converter With Consideration of Internal Harmonic Dynamics," *IEEE Trans. Power Electron.*, vol. 34, no. 3, pp. 2134-2148, March 2019.

[13] C. Zhang, M. Molinas, S. Fyen, J. A. Suul and I. Takanori, "Harmonic Domain SISO Equivalent Impedance Modeling and Stability Analysis of a Single-phase Grid Connected VSC," *IEEE Trans. Power Electron.*, to be published, doi: 10.1109/TPEL.2020.2970390.

[14] B. Wen, D. Boroyevich, R. Burgos, P. Mattavelli and Z. Shen, "Inverse Nyquist Stability Criterion for Grid-Tied Inverters," *IEEE Trans. Power Electron.*, vol. 32, no. 2, pp. 1548-1556, Feb. 2017.

[15] Z. Liu, J. Liu, W. Bao and Y. Zhao, "Infinity-Norm of Impedance-Based Stability Criterion for Three-Phase AC Distributed Power Systems With Constant Power Loads" *IEEE Trans. Power Electron.*, vol. 30, no. 6, pp. 3030-3043, June 2015.

[16] A. Riccobono and E. Santi, "Comprehensive Review of Stability Criteria for DC Power Distribution Systems," *IEEE Trans. Ind. Appl.*, vol. 50, no. 5, pp. 3525-3535, Sept.-Oct. 2014.

[17] S. D. Sudhoff, S. F. Glover, P. T. Lamm, D. H. Schmucker, and D. E. Delisle, "Admittance space stability analysis of power electronic systems," *IEEE Trans. Aerosp. Electron.*, vol. 36, no. 3, pp. 965-973, Jul. 2000.

[18] Q. Yan, B. Zhang and M. Kezunovic, "Optimized Operational Cost Reduction for an EV Charging Station Integrated with Battery Energy Storage and PV generation," *IEEE Trans. Smart Grid,* vol. 10, no. 2, pp. 2096-2106, March 2019.

[19] M. Rasheduzzaman, J. A. Mueller and J. W. Kimball, "Reduced-Order Small-Signal Model of Microgrid Systems," *IEEE Trans. Sustain. Energy*, vol. 6, no. 4, pp. 1292-1305, Oct. 2015.

[20] A. A. A. Radwan and Y. A. R. I. Mohamed, "Analysis and Active-Impedance-Based Stabilization of Voltage-Source-Rectifier Loads in Grid-Connected and Isolated Microgrid Applications," *IEEE Trans. Sustain. Energy*, vol. 4, no. 3, pp. 563-576, July 2013.

[21] Shuoh Rern, P. T. Kabamba and D. S. Bernstein, "Guardian map approach to robust stability of linear systems with constant real parameter uncertainty," *IEEE Trans. Automat. Contr.*, vol. 39, no. 1, pp. 162-164, Jan. 1994.

[22] R. Wang, Q. Sun, Y. Gui and D. Ma, "Exponential-function-based droop control for islanded microgrids," *J. Mod. Ppwer Syst. Cle.*, vol. 7, no. 4, pp. 899-912, July 2019.

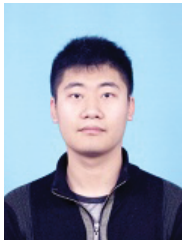

Wang Rui received the B.S. degree in electrical engineering and automation in 2016 from Northeastern University, Shenyang, China, where he is currently working toward the Ph.D. degree in power electronics and power drive. Since 2019, he has become a visiting scholar with the Energy Research Institute, Nanyang Technological University, Singapore. He has authored or coauthored over 30 papers, authorized over 10 invention patents. His research interest focuses on collaborative optimization of distributed generation and its stability analysis of electromagnetic timescale in Energy Internet.

Sun Qiuye (M'11,SM'19) received the Ph.D. degree in 2007. He is currently a full Professor with Northeastern University and obtained Special Government Allowances from the State Council in China. He has authored or coauthored over 200 papers, authorized over 100 invention patents, and published over 10 books or textbooks. He is an Associate Editor of *IEEE Transactions on Neural Networks and Learning Systems*, *IET Cyber-Physical Systems*, *CSEE Journal of Power and Energy Systems*, *IEEE/CAA Journal of Automatica Sinica*, *Journal of Control and Decision* and so on. His current research interests include optimization analysis technology of power distribution network, network control of Energy Internet, Integrated Energy Systems and Microgrids.

Dazhong Ma (M'16) received the B.S. degree in automation in 2004 and the Ph.D. degree in control theory and control engineering in 2011, from Northeastern University, Shenyang, China, where he is currently an Associate Professor.

His current research interests include fault diagnosis, fault-tolerant control, energy management systems, control and optimization of distributed generation systems, microgrids, and energy Internet.

Qin Dehao received the B.S. degree and M.Sc. degree in Northeastern University, Shenyang, China, in 2017 and 2020, respectively, all with provincial outstanding graduate. He is currently pursuing the Ph.D degree in the Clemson University Restoration Institute, Clemson University, South Carolina, USA. His current research interests include bidirectional DC-DC converter, SiC-based power electronics, etc.

Gui Yonghao (S'11-M'17) received the B.S. degree in automation from Northeastern University, Shenyang, China, in 2009. He received the M.S. and Ph.D. degrees in electrical engineering from Hanyang University, Seoul, South Korea, in 2012 and 2017, respectively. From February 2017 to November 2018, he worked with the Department of Energy Technology, Aalborg University, Aalborg, Denmark, as a Postdoctoral Researcher. Since December 2018, he has been working with the Automation & Control Section, Department of Electronic Systems, Aalborg University, Aalborg, Denmark, where he is currently an Assistant Professor. His research interests include control of Power Electronics in Power Systems, Energy Internet, and Smart Grids. Dr. Gui serves as an Associate Editor for the *IEEE Access* and the *International Journal of Control, Automation and Systems*. He was a recipient of the IEEE Power and Energy Society General Meeting Best Conference Paper Award in 2019.

Wang Peng (F'18) received the B.Sc. degree in electronic engineering from Xian Jiaotong University, Xian, China, in 1978, the M.Sc. degree from Taiyuan University of Technology, Taiyuan, China, in 1987, and the M.Sc. and Ph.D. degrees in electrical engineering from the University of Saskatchewan, Saskatoon, SK, Canada, in 1995 and 1998, respectively. Currently, he is a full Professor with the School of Electrical and Electronic Engineering at Nanyang Technological University, Singapore. He is an Associate Editor or Guest Editor-in-Chief of *IEEE Transactions on Smart Grid*, *IEEE Transactions on Power Delivery*, *Journal of Modern Power Systems and Clean Energy*, *CSEE Journal of Power and Energy Systems*, and so on. His current research interests include power system planning and operation, renewable energy planning, solar/electricity conversion system and power system reliability analysis.